

# Armchair graphene nanoribbons: Electronic structure and electric field modulation

Hassan Raza, Edwin C. Kan

*School of Electrical and Computer Engineering, Cornell University Ithaca NY 14853 USA*

We report electronic structure and electric field modulation calculations in the width direction for armchair graphene nanoribbons (acGNRs) using a semi-empirical extended Hückel theory. Important band structure parameters are extracted, *e.g.* effective masses, velocities and band gaps *etc.* It is proposed to divide acGNRs into three categories, where the corresponding  $p_z$  orbital tight-binding parameters are extracted if feasible. Furthermore, the effect of electric field in the width direction on acGNRs dispersion is numerically explored. It is shown that for certain acGNRs, an external electric field can turn a semiconducting acGNR to metallic.

PACS numbers: 73.22.-f, 73.20.-r, 72.80.Rj

## I. INTRODUCTION

Unconstrained Graphene is a two dimensional hexagonal monolayer of carbon atoms. Its unique linear dispersion around the Dirac point and zero band gap [1, 2] has generated significant interest [3]. Constraining one dimension of graphene results into nanoribbons. The electronic structure of these graphene nanoribbons (GNR) depends on the width and chirality [4, 5, 6, 7, 8, 9, 10, 11]. Two unique GNRs are armchair and zigzag referred to as acGNR and zzGNR in this article. acGNR has an armchair edge as shown in Fig. 1 and when conceptually rolled to form a nanotube results in a zigzag tube and *vice versa*. Some experimental techniques have already been used to measure their properties [12] and numerous fabrication schemes have been devised [14, 15, 16]. Elec-

tronic applications of graphene and GNRs are also being sought after [17, 18, 19].

In acGNRs, the wavefunctions associated with bands around Fermi energy are distributed throughout the width of the nanoribbon. However in zzGNRs, the wavefunctions for such bands are localized at the edges [4, 5]. In addition, the bands around the Fermi energy have very small dispersion that leads to Stoner magnetism in these edge states [4, 5]. These spin polarized bands can be modulated with an external electric field in the width direction, resulting in some interesting ideas [20]. In contrast, due to quantization in one direction, acGNRs have velocities less than found in unconstrained graphene sheets and the band structure has a parabolic character around the band edge within few tens of meV.

In this paper, we focus on acGNR and study their electronic structure and electric field modulation in the width direction with a semi-empirical extended Hückel theory (EHT). The detailed model has been reported in Ref. [8]. EHT parameters are transferable and have been benchmarked with generalized gradient approximation of density functional theory for carbon atoms in graphene structure. EHT is computationally inexpensive and hence appropriate for calculating properties of large systems without compromising accuracy. As an example, up to about 1000 atoms electronic structure calculations [21] and up to about 200 atoms transport calculations [22] have been reported in silicon based systems with modest computational resources. In this paper, up to about 160 atoms calculations are presented. Contributions from five nearest neighbors are included. C-C atomic distance is taken as  $1.44\text{\AA}$ , for which EHT parameters have been optimized. Further structural relaxation is ignored. Atomic visualization is done using GaussView [23].

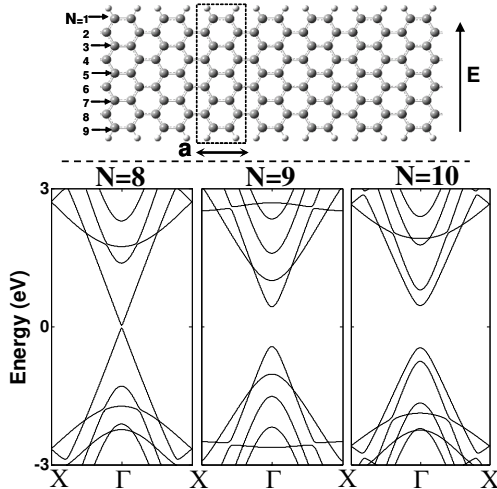


FIG. 1: Electronic structure of armchair graphene nanoribbons (acGNR). The ball and stick model of a graphene nanoribbon with  $N=9$  is shown with the unit cell. E-k diagrams are shown for three different types of acGNRs using extended Hückel theory (EHT).  $N=8,11,14,\dots$  acGNRs have very small band gap. We call these  $\alpha$ -acGNRs in this article.  $N=9,12,15,\dots$  acGNRs are semiconducting with band gap and are referred to as  $\beta$ -acGNRs.  $N=10,13,16,\dots$  acGNRs are also semiconducting and we call them  $\gamma$ -acGNRs.

## II. ELECTRONIC STRUCTURE

On a  $p_z$  level of the tight-binding theory, two-third acGNRs are semiconducting with a band gap inversely proportional to their widths and the others are metallic depending on the chirality [4]. However, one obtains a different result using a more sophisticated theory [24].

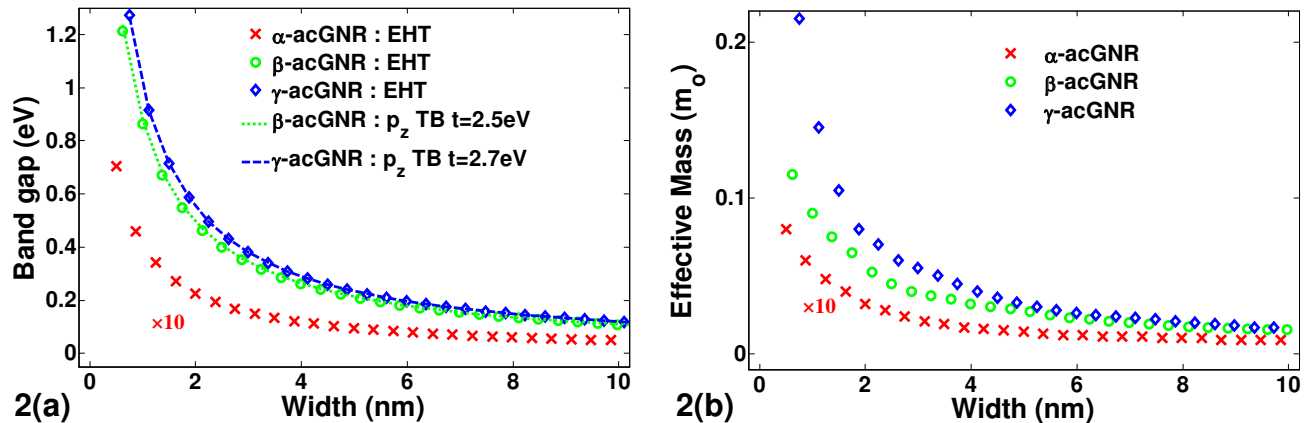


FIG. 2: (color online) Band gaps and effective masses. (a) Variation of band gap with nanoribbon widths of different types of acGNRs. Band gap for  $\alpha$ -acGNRs varies as  $0.046eV/W(nm)$ , for  $\beta$ -acGNRs varies as  $0.97eV/W(nm)$  and for  $\gamma$ -acGNRs varies as  $1.14eV/W(nm)$ . Using a  $p_z$ -orbital tight binding method,  $t=2.5eV$  and  $t=2.7eV$  match the band gaps obtained by extended Hückel theory (EHT) for  $\beta$ -acGNRs and  $\gamma$ -acGNRs, respectively.

First, the metallic acGNRs also have a small band gap that is inversely proportional to the width. Second, the remaining semiconducting acGNRs only follow an inverse relation within its own category. For convenience, we propose to categorize them into  $\alpha$ -,  $\beta$ - and  $\gamma$ -acGNRs. This classification is similar to the ones recently used recently in Refs. [24, 25].  $\alpha$ -acGNRs are  $N=8,11,14,\dots$  and have very small band gap.  $\beta$ -acGNRs are  $N=9,12,15,\dots$  and  $\gamma$  acGNRs are  $N=10,13,16,\dots$  acGNRs have also been classified into three subclasses in context of the orbital diamagnetism [6].

An electronic structure calculation for each type of acGNR is shown in Fig. 1. As can be seen that  $N=8$   $\alpha$ -acGNR has a small band gap and near band edge has a nonlinear dispersion. Furthermore,  $N=9$   $\beta$ -acGNR has a large band gap with a parabolic dispersion around band edge. Interestingly,  $N=10$   $\gamma$ -acGNR has a slightly larger band gap with larger effective mass dispersion around band edge and smaller velocity as compared to  $N=9$   $\beta$ -acGNR. We extract the band gaps and effective masses within few tens of meV around the band edges of these three types of acGNRs and plot them in Fig. 2(a) and (b), respectively. Fig. 2(a) is a computational verification of earlier results [24] on a semi-empirical level. For each type of acGNR, band gaps and effective masses are inversely proportional to the width with a different proportionality constant. The band gap *versus* width ( $W$ ) relations are given as:

$$E_{gap} = \begin{cases} 0.046eV/W(nm) & \text{for } \alpha - acGNR \\ 0.970eV/W(nm) & \text{for } \beta - acGNR \\ 1.140eV/W(nm) & \text{for } \gamma - acGNR \end{cases}$$

We find Fig. 2(b) important because some approaches toward graphene structures involve effective mass description [18]. Each type of acGNRs follow an inverse relation

of effective mass with the width given below:

$$\frac{m}{m_o} = \begin{cases} 0.005/W(nm) & \text{for } \alpha - acGNR \\ 0.091/W(nm) & \text{for } \beta - acGNR \\ 0.160/W(nm) & \text{for } \gamma - acGNR \end{cases}$$

where  $m_o$  is the free electron mass. Furthermore, we determine the correct  $p_z$ -orbital tight binding parameters that reproduce the band gaps as shown in Fig. 2(a). These parameters are 2.5eV and 2.7eV for  $\beta$ - and  $\gamma$ -acGNRs respectively. Since tight-binding parameter for  $\gamma$ -acGNRs is higher, we conclude that wavefunctions are hybridized more in this type of acGNR. This physical effect has some implications for electric field modulation as discussed in next section.

### III. ELECTRIC FIELD MODULATION

Fig. 3(a) shows electric field modulation of the band structure for an  $N=10$  acGNR. The effective mass around  $\Gamma$ -point increases with increasing electric field ( $E$ ). Furthermore, for  $E=0$ , the band dispersion shows velocity very close to the unconstrained graphene velocity ( $=8.8 \times 10^5$  m/sec) indicated by red (grey) circles. With increasing  $E$ , velocity decreases to about  $5 \times 10^5$  m/sec. In addition, the band widths of the valence and conduction bands are also decreasing. Moreover, a 'mexican hat' structure is observable that has been seen in graphene bilayers [21, 26, 27]. We show the extracted effective masses around  $\Gamma$ -point for  $N=8, 9$  and  $10$ , which are  $\alpha$ -,  $\beta$ - and  $\gamma$ -acGNRs, respectively in Fig. 3(b). These effective masses are valid for tenths of  $k_B T$  for  $\alpha$ -acGNRs and for a few  $k_B T$  for  $\beta$ - and  $\gamma$ -acGNRs. After this energy scale, the band dispersions become linear again and remain so for about a few electron volts when they become nonlinear and hence saturate as shown in Fig. 3(a).

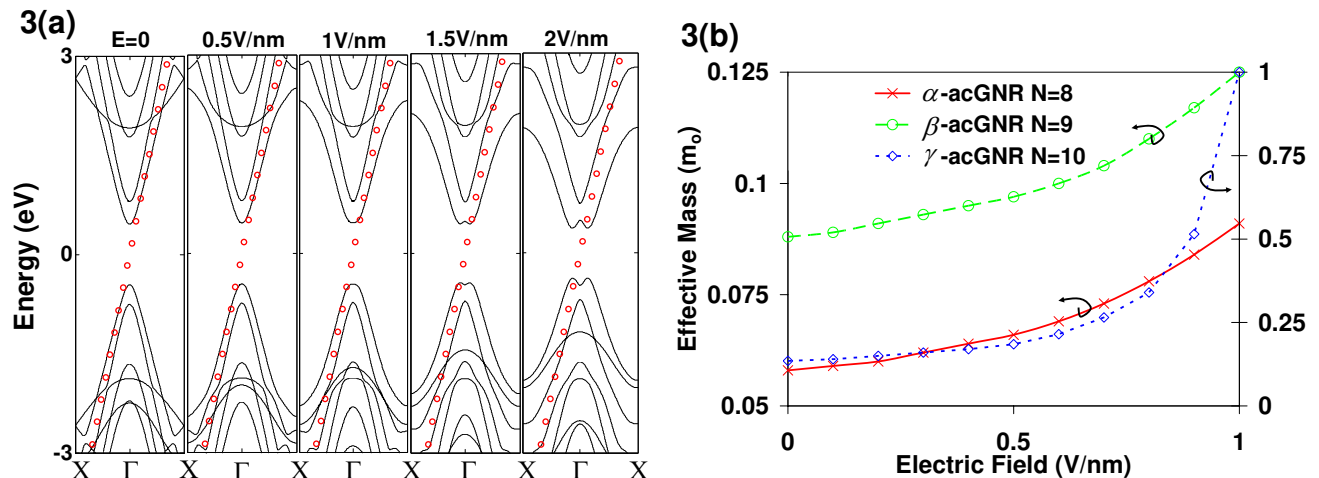


FIG. 3: (color online) Electric field modulation of band dispersions. (a) Variation of velocity with electric field in the width direction. The linear dispersion shown by red circles represents a value of  $8.8 \times 10^5$  m/s - velocity around the Dirac point for graphene calculated using EHT. (b) Variation of effective masses with electric field in the width direction. Effective masses are obtained by parabolic fits to the conduction bands within a few  $kT$  of band edge for  $\beta$ -acGNRs and  $\gamma$ -acGNRs, and within a fraction of a  $kT$  for  $\alpha$ -acGNRs.

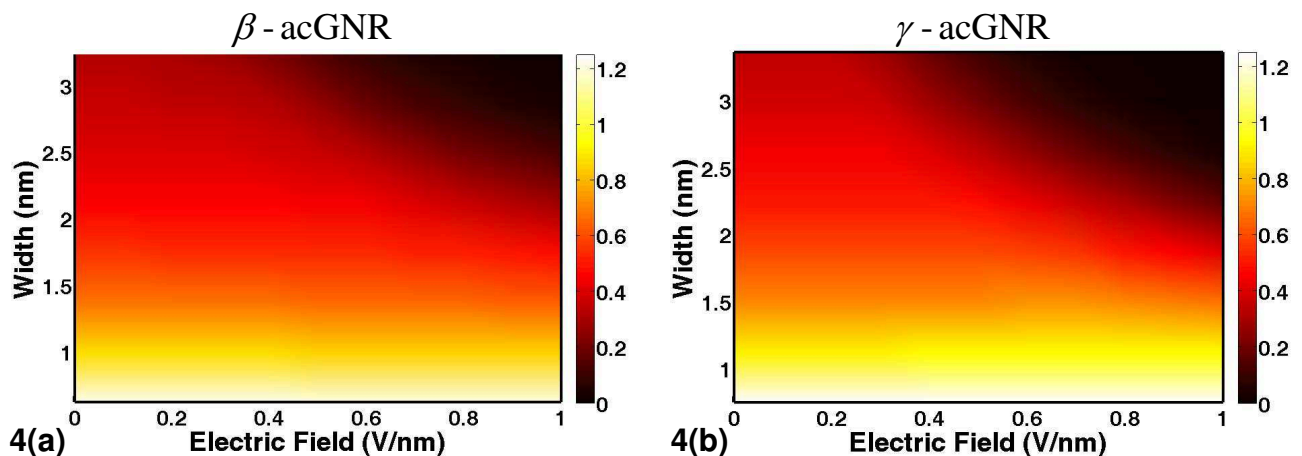


FIG. 4: (color online) Band gap modulation with electric field. (a) Band gap as a function of width and electric field for  $\beta$ -acGNRs. (b) Band gap as a function of width and electric field for  $\gamma$ -acGNRs.  $\gamma$ -acGNRs have larger band gap modulation as compared to  $\beta$ -acGNRs. The width has discrete values. The continuous variation is for visualization only.

1V/nm electric field is within the dielectric breakdown limit of thermal  $\text{SiO}_2$ , which may result in higher electric field inside graphene due to smaller dielectric constant. Moreover, high-K dielectrics can be used to further enhance the electric field. However, such a high electric field may lead to dielectric reliability issues and is undesirable.

Moreover, the band gap is also decreasing with increasing electric field. One clear feature is the location of wavevector corresponding to the conduction/valence band minimum/maximum. These two perturbations in the band structure are further explored in Figs. 4 and 5 respectively for  $\beta$ - and  $\gamma$ -acGNRs. The continuum visualization for vertical axis is for visualization only, since

the nanoribbon width has discrete values. In Fig. 4, we show band gap modulation as a function of width and electric field.  $\gamma$ -acGNRs have larger band gap modulation as compared to  $\beta$ -acGNRs. This is consistent because wavefunctions are more hybridized in  $\gamma$ -acGNRs and hence any perturbation affects the band structure more than  $\beta$ -acGNRs. Furthermore, with appropriate electric field applied, one can convert a semi-conducting acGNR into a metallic one. This feature can be utilized in future novel devices. In order to change the band structure, one has to incorporate perturbation on the order of the tight-binding parameter (2.5eV for  $\beta$ - and 2.7eV for  $\gamma$ -acGNRs). Therefore, an electric field of 1V/nm should not be able to induce a significant change

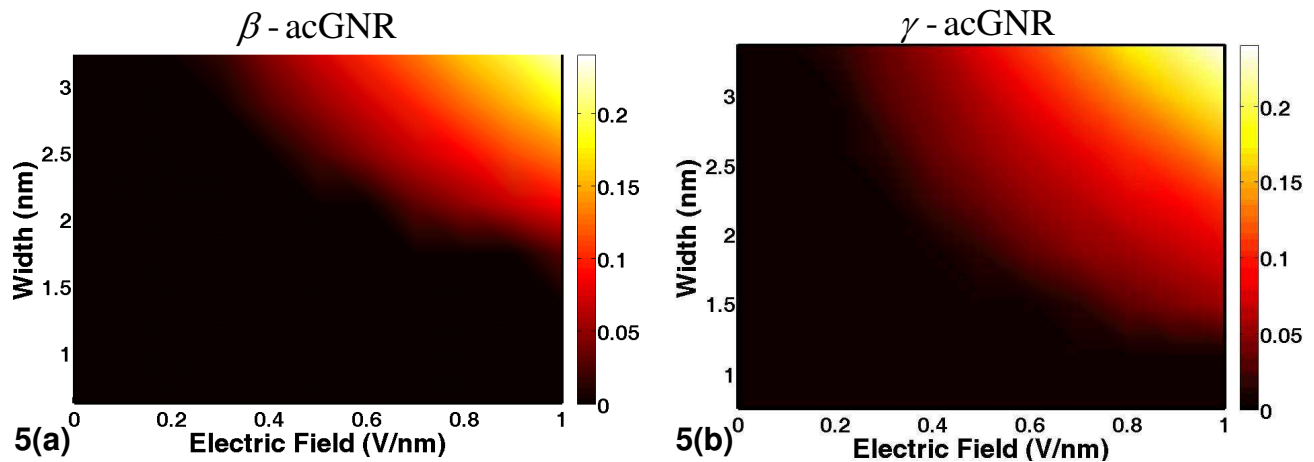


FIG. 5: (color online) The wavevector corresponding to band edge ( $k_{BE}$ ) modulation with electric field. (a)  $k_{BE}$  as a function of width and electric field for  $\beta$ -acGNRs.  $k_{BE}$  is the value of  $k$  wavevector at conduction/valence band minimum/maximum. (b)  $k_{BE}$  as a function of width and electric field for  $\gamma$ -acGNRs. The value of  $k$  at X point is about  $0.727\text{\AA}^{-1}$ . Similar to band gap modulation in Fig. 4,  $\gamma$ -acGNRs have larger shift in  $k_{BE}$  than  $\beta$ -acGNRs.

in small width acGNRs due to small perturbation as shown in Fig. 4. However, the same electric field can change the electronic structure of a wider acGNRs due to larger potential variation. Furthermore, in Fig. 5, we show the wavevector shift ( $k_{BE}$ ) corresponding to conduction band minimum/valence band maximum. Again,  $\gamma$ -acGNRs have larger shift as compared to  $\beta$ -acGNRs. Overall, this shift can be as much as one third of the wavevector at X point. Unfortunately, we could not find a consistent set of  $p_z$ -orbital tight-binding parameters to reproduce Figs. 3, 4 and 5.

#### IV. CONCLUSIONS

We have studied band structure and electric field modulation of acGNRs. We propose to categorize them into

three types, which exhibit distinct electronic structure and electric field modulation properties. We extract important band structure parameters and propose a set of  $p_z$ -orbital tight-binding parameters benchmarked with extended Hückel theory to reproduce correct band gaps for different types of acGNRs.

The work is supported by National Science Foundation (NSF) and by Nanoelectronics Research Institute (NRI) through Center for Nanoscale Systems (CNS) at Cornell University. We are grateful to Tehseen Raza for GaussView [23] visualizations and for reviewing the manuscript.

- 
- [1] P. R. Wallace, Phys. Rev. **71**, 622 (1947).
  - [2] R. Saito, G. Dresselhaus and M.S. Dresselhaus, "Physical Properties of Carbon Nanotubes", (Imperial College Press, London, UK, 1998).
  - [3] A. K. Geim and K. S. Novoselov, Nature Materials **6**, 183 (2007).
  - [4] K. Nakada, M. Fujita, G. Dresselhaus and M. S. Dresselhaus, Phys. Rev. B **54**, 17954 (1996).
  - [5] M. Fujita, K. Wakabayashi, K. Nakada and K. Kusakabe, J. Phys. Soc. of Japan **65**, 1920 (1996).
  - [6] K. Wakabayashi, M. Fujita, H. Ajiki and M. Sigrist, Phys. Rev. B **59** 8271 (1999).
  - [7] T. Kawai, Y. Miyamoto, O. Sugino and Y. Koga, Phys. Rev. B **62**, R16349 (2000).
  - [8] H. Raza and E. C. Kan, accepted in J. of Comp. Elec. (<http://www.springerlink.com/content/k07807207x36315w/>)
  - [9] V. Barone, O. Hod and G. E. Scuseria, Nano. Lett. **6**, 2748 (2006).
  - [10] Z. Chen, Y.-M. Lina, M. J. Rooksa and P. Avouris, Physica E: Low-dimensional Systems and Nanostructures **40**, 228 (2007).
  - [11] L. Brey and H. A. Fertig, Phys. Rev. B **73**, 235411 (2006).
  - [12] M. Y. Han, B. Ozyilmaz, Y. Zhang and P. Kim, Phys. Rev. Lett. **98**, 206805 (2007).
  - [13] T. Enoki, Y. Kobayashi and K.-I. Fukui, Int. Rev. in Phys. Chem. **26**, 609 (2007).
  - [14] X. Li, X. Wang, L. Zhang, S. Lee, H. Dai, Science **319**, 1229 (2008).
  - [15] K. S. Novoselov, A. K. Geim, S. V. Morozov, D. Jiang, Y. Zhang, S. V. Dubonos, I. V. Grigorieva, and A. A. Firsov, Science **306** 666 (2004).
  - [16] C. Berger, Z. Song, X. Li, X. Wu, N. Brown, C. Naud, D.

- Mayou, T. Li, J. Hass, A. N. Marchenkov, E. H. Conrad, P. N. First and W. A. de Heer, *Science* **312** 1191 (2006).
- [17] G. Fiori, G. Iannaccone, *IEEE Elec. Dev. Lett.* **28**, 760 (2007).
- [18] G. Liang, N. Neophytou, D. E. Nikonov and M. S. Lundstrom, *IEEE Trans. Electron Devices* **54**, 677 (2007).
- [19] G. Gua, S. Nie, R. M. Feenstra, R. P. Devaty and W. J. Choyke, W. K. Chan and M. G. Kane, *Appl. Phys. Lett.* **90**, 253507 (2007).
- [20] Y.-W. Son, M. L. Cohen, S. G. Louie, *Nature* **444**, 347 (2006).
- [21] H. Raza, *Phys. Rev. B* **76**, 045308 (2007).
- [22] H. Raza, in preparation (2008).
- [23] R. Dennington II, T. Keith, J. Millam, K. Eppinnett, W. L. Hovell and R. Gilliland, *GaussView, Version 3.0* (Semichem, Inc., Shawnee Mission, KS, 2003).
- [24] Y.-W. Son, M. L. Cohen, S. G. Louie, *Phys. Rev. Lett.* **97**, 216803 (2006).
- [25] B. Sahu, H. Min, A. H. MacDonald, S. K. Banerjee, *condmat/0801.1991* (2008).
- [26] H. Min, B. Sahu, S. K. Banerjee and A. H. MacDonald, *Phys. Rev. B* **75**, 155115 (2007).
- [27] E. V. Castro, K. S. Novoselov, S.V. Morozov, N. M. R. Peres, J. M. B. Lopes dos Santos, Johan Nilsson, F. Guinea, A. K. Geim and A. H. Castro Neto, *Phys. Rev. Lett.* **99**, 216802 (2007).